Anticodon Domain Modifications Contribute Order to tRNA for Ribosome-Mediated Codon Binding[†,‡]

Franck A. P. Vendeix,[§] Agnieszka Dziergowska,[||] Estella M. Gustilo,[§] William D. Graham,[§] Brian Sproat,[⊥] Andrzej Malkiewicz,[||] and Paul F. Agris*[,§]

Department of Molecular and Structural Biochemistry, North Carolina State University, 128 Polk Hall, Raleigh, North Carolina 27695-7622, Institute of Organic Chemistry, Technical University, Zeromskiego 116, 90-924 Lŏdü, Poland, and Integrated DNA Technologies BVBA, Provisorium 2, Minderbroedersstraat 17-19, B-3000 Leuven, Belgium

Received November 29, 2007; Revised Manuscript Received March 11, 2008

ABSTRACT: The accuracy and efficiency with which tRNA decodes genomic information into proteins require posttranscriptional modifications in or adjacent to the anticodon. The modification uridine-5-oxyacetic acid (cmo^5U_{34}) is found at wobble position 34 in a single isoaccepting tRNA species for six amino acids, alanine, leucine, proline, serine, threonine, and valine, each having 4-fold degenerate codons. cmo^5U_{34} makes possible the decoding of 24 codons by just six tRNAs. The contributions of this important modification to the structures and codon binding affinities of the unmodified and fully modified anticodon stem and loop domains of $tRNA^{Val3}_{UAC}$ (ASL^{Val3}_{UAC}) were elucidated. The stems of the unmodified ASL^{Val3}_{UAC} and that with cmo^5U_{34} and N^6-methyladenosine, m^6A_{37}, adopted an A-form RNA conformation (rmsd ~ 0.6 Å) as determined with NMR spectroscopy and torsion-angle molecular dynamics. However, the UV hyperchromicity, circular dichroism ellipticity, and structural analyses indicated that the anticodon modifications enhanced order in the loop. ASL^{Val3}_{UAC}-cmo^5U_{34};m^6A_{37} exhibited high affinities for its cognate and wobble codons GUA and GUG, and for GUU in the A-site of the programmed 30S ribosomal subunit, whereas the unmodified ASL^{Val3}_{UAC} bound less strongly to GUA and not at all to GUG and GUU. Together with recent crystal structures of ASL^{Val3}_{UAC}-cmo^5U_{34};m^6A_{37} bound to all four of the valine codons in the A-site of the ribosome's 30S subunit, these results clearly demonstrate that the xo^5U_{34}-type modifications order the anticodon loop prior to A-site codon binding for an expanded codon reading, possibly reducing an entropic energy barrier to codon binding.

Transfer RNA is one of the most understood biological macromolecules. The relationship of its nucleoside chemistry and oligonucleotide structure to its functions in protein synthesis has been studied extensively (*1, 2*). Those studies have led to the identification of more than 70 different posttranscriptional modifications present in tRNAs (*3*). tRNA modifications increase stability (*4*), enhance decoding (*5*), restore ribosomal binding (*6*), and influence reading frame maintenance (*7, 8*). In the course of translation, anticodon domain modifications in particular play important roles in the accuracy and efficiency of protein synthesis. Therefore, the modifications that occur at anticodon wobble position 34, and at the conserved purine 37, 3′-adjacent to the anticodon, are of obvious interest in tRNA's decoding of mRNA (Figure 1). These modifications play critical and distinctive roles in tRNA's accurate and efficient binding of cognate and wobble codons within the ribosome's A-site (*9*).

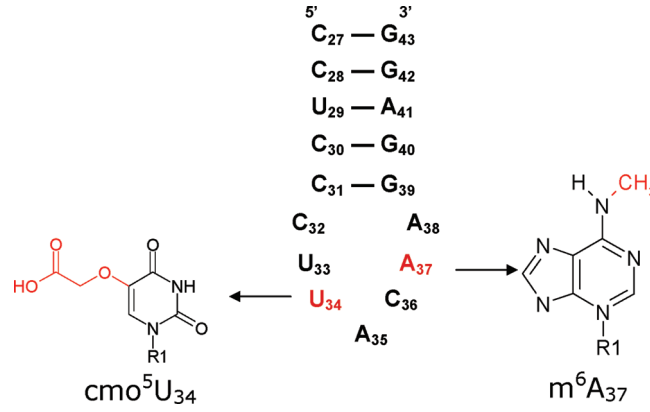

FIGURE 1: Nucleotide sequence of the *Escherichia coli* $tRNA^{Val3}_{UAC}$ anticodon stem and loop (ASL^{Val3}_{UAC}) and its modified nucleosides. The nucleotide sequence and secondary structure of the ASL^{Val3}_{UAC} has two modifications, uridine-5-oxyacetic acid at wobble position 34 (cmo^5U_{34}) and N^6-methyladenosine at position 37 (m^6A_{37}). The oxyacetic acid is dissociated at physiological pH. The oxyacetic acid and methyl groups are colored red.

Some 40 years ago, Francis Crick explained how a limited number of tRNAs could decode the 61 amino acid codons

[†] This work was supported by grants from the National Institutes of Health (Grant 2-RO1-GM23037 to P.F.A.), the National Science Foundation (Grants MCB-0548602 and 2-RO1-GM23037 to P.F.A.), RNA-TEC NV, and the Polish Ministry of Science and Education (to A.M.).

[‡] The coordinates of the 10 lowest-energy structures and the average structures have been deposited and are available from the Protein Data Bank as entries 2JR4 for unmodified ASL^{Val3}_{UAC} and 2JRG for ASL^{Val3}_{UAC}-cmo^5U_{34};m^6A_{37}.

* To whom correspondence should be addressed. Phone: (919) 515-6188. E-mail: Paul_Agris@ncsu.edu. Fax: (919) 515-2047.

[§] North Carolina State University.

[||] Technical University.

[⊥] Integrated DNA Technologies BVBA.

10.1021/bi702356j CCC: $40.75
Published on Web 05/13/2008

(*10*). Our view of codon recognition by tRNA was then altered in the modified wobble hypothesis to accommodate new information about modifications (*11*). The limited number of tRNAs requires most tRNAs to read more than one codon. Some tRNAs respond to codons in "mixed" codon boxes where distinction of the third codon base (the most degenerate of coding positions) is important for discriminating between the correct cognate or wobble codons and the incorrect but near-cognate codons. For example, a wobble position, 2-thiouridine 34 (s^2U_{34}), enables recognition of the canonical third codon nucleotide A3 and will wobble to G3 but will not recognize either U3 or C3 (*10, 12*). In contrast, other modification chemistries expand wobble codon recognition, such as tRNA's wobble position inosine 34 (I_{34}) that will bind codons ending in A3, C3, or U3 (*12*).

Modifications expand tRNA's codon recognition beyond that envisioned in the wobble hypothesis. Crick suggested that a U_{34} would pair with an A and wobble to a G in the third position of the codon (A3 or G3) but would not base pair with a U3 or C3. He argued that a U_{34} paired with a U3 or C3 would markedly distort the anticodon−codon minihelix (*10*). However, wobble position U_{34} of some tRNA species will base pair with a U3 and even a C3 in recognizing all of the synonymous codons of a 4-fold degenerate codon box (*9, 13–16*). For tRNAs to recognize codons ending with a U3 or C3, as well as codons ending with A3 and G3, modification of wobble position U_{34} is essential (*9, 13–16*). The modified nucleoside capable of binding to A, G, U, and C is uridine-5-oxyacetic acid, cmo^5U_{34}[1] (Figure 1). Each of the six amino acids, alanine, leucine, proline, serine, threonine, and valine, having 4-fold degenerate codons, has a single isoaccepting tRNA species containing the modification cmo^5U_{34} (*17*), but would a tRNA species with cmo^5U_{34} be sufficient for cell viability in the absence of all other isoaccepting tRNAs in vivo? The function of cmo^5U_{34} in $tRNA^{Pro}$ was analyzed by introducing null copies of the two genes (*cmoA* and *cmoB*) identified as part of the cmo^5U_{34} synthetic pathway into a strain of *Salmonella* having only one of three $tRNA^{Pro}$ isoacceptors, that with the wobble cmo^5U_{34} modification (*18*). Growth of this and other mutant strains demonstrated that all four proline codons (CCU/C/A/G) were read by the cmo^5U-containing $tRNA^{Pro}$, and that the complete modification was critical for reading codons ending in U and C (*18*). However, the physicochemical contributions of cmo^5U_{34} to anticodon−codon recognition were not known, though a study of mononucleotide conformation suggested that cmo^5U_{34} favored the C2′-*endo* sugar conformation due to an interaction between the modification's free acid and the 5′-phosphate backbone (*15*).

We had determined that the cmo^5U_{34} modification was required for translocation of $tRNA^{Val3}_{UAC}$ from the ribosome's A-site to its P-site when bound to the GUU codon but was not required when it was bound to the cognate codon GUA (*19*). Surprisingly, the insertion of the single cmo^5U_{34} modification allowed translocation. The absence of N^6-methyladenosine, m^6A_{37}, which is also a modification found in native $tRNA^{Val3}_{UAC}$, did not alter the translocation of unmodified $tRNA^{Val3}_{UAC}$ on its cognate codon and confirmed that modifications of purine 37 are not required for translocation on the cognate codon. Thus, results from studies *in vivo* and *in vitro* confirmed the importance of the cmo^5U_{34} modification in tRNAs for the six amino acids, and the decoding of the corresponding 18−24 codons. However, the chemical and structural contributions of cmo^5U_{34} to $tRNA^{Val3}_{UAC}$ function were unknown. To understand how cmo^5U_{34} could affect function, we report the solution structures of the unmodified and fully modified anticodon stem and loop domains of $tRNA^{Val3}_{UAC}$ (ASL^{Val3}_{UAC}) and compare them to the crystal structures of the ASL^{Val3}_{UAC}-cmo^5U_{34};m^6A_{37} bound to its four valine codons in the decoding site of the ribosome's 30S subunit. In addition, we report the thermodynamic and A-site codon binding properties of the unmodified ASL^{Val3}_{UAC} and modified ASL^{Val3}_{UAC}-cmo^5U_{34};m^6A_{37}. We observed that cmo^5U_{34} and m^6A_{37} in ASL^{Val3}_{UAC} confer order and stability to prestructure the tRNA before binding to the codon in the ribosome's A-site.

EXPERIMENTAL PROCEDURES

RNA Sample Preparation. The unmodified *Escherichia coli* ASL^{Val3}_{UAC} used in this study was chemically synthesized by Dharmacon (ThermoFisher, Lafayette, CO) using "ACE" chemistry (*20*). The modified ASL^{Val3}_{UAC} construct was synthesized by Integrated DNA Technologies BVBA (formerly RNA-Tec). For the solid-phase synthesis of the modified ASL^{Val3}_{UAC}, the unmodified and modified phosphoramidite monomers were protected by 5′-*O*-dimethoxytrityl and 2′-*O*-*tert*-butyldimethylsilyl groups, whereas the exoamine groups were protected with 4-*tert*-butylphenoxyacetyl groups. The cmo^5U carboxylic acid moiety was protected as its *p*-nitrophenylethyl ester. The deprotection of the oligomers has been achieved (*21*). The ASLs were purified by HPLC using a Nucleogen 60-7 DEAE (250 mm × 10 mm) column. Desalting was accomplished with Waters Corp. Sep-pak cartridges. For purposes of crystallography and NMR spectroscopy, the ASLs were further purified by extensive dialysis (using Slide-A-Lyzer MINI Dialysis Units, 3.5K MWCO from Pierce) against 20 mM phosphate buffer (pH 6.2), 50 mM Na^+, and 50 mM K^+. After the pH had been adjusted to 6.2 (pH/Ion Analyzer MA 235, Mettler Toledo), the oligonucleotides were heated to 80 °C followed by slow cooling to form a solution homogeneous in ASL conformation. After cooling, the samples were lyophilized using a freeze-dryer (Thermo Savant SPD Speed Vac, Thermo Scientific) and then dissolved in 99.996% ^2H_2O or a 90% ^1H_2O/10% ^2H_2O mixture to give a final volume of 300 μL. Samples in ^2H_2O were redissolved in ^2H_2O at least twice more and lyophilized. NMR samples of the ASLs were generally at concentrations of 2 mM (in ^1H_2O) and 1.5 mM (in ^2H_2O). In addition to HPLC nucleoside composition analyses (*22*), mass spectroscopy (MALDI-TOF), and NMR analyses, the results of X-ray crystallography unambiguously confirmed the incorporation of m^6A_{37} and cmo^5U_{34} into the ASLs.

Ribosomal Binding Assay. The 27-mer mRNA sequences used in codon binding assays were designed from that of T4 gp32 mRNA (*23*), purchased from Dharmacon, chemi-

[1] Abbreviations: ASL, anticodon stem and loop domain; ASL^{Val3}_{UAC}, ASL of *Escherichia coli*'s valine tRNA isoaccepting species 3 with anticodon UAC; CD, circular dichroism spectropolarimetry; cmo^5U_{34}, uridine-5-oxyacetic acid; HPLC, high-performance liquid chromatography; m^6A_{37}, N^6-methyladenosine 37; NOE, nuclear Overhauser effect; T_m, temperature at the midpoint in the UV-monitored, major thermal transition.

cally deprotected, and HPLC-purified. Each mRNA sequence was entered into mFold (*33*) to ensure that there was a low probability it would fold into a stable conformation. The mRNA sequences were 5′-GGCAAGGAGGUAAAAAUGG-UAGCACGU-3′, 5′-GGCAAGGAGGUAAAAAUGGUGG-CACGU-3′, 5′-UGCAAGGAGGUAAAAAUGGUCGCA-CGU-3′, and 5′-UUGAAGGAGGGUUUUAUGGUUGC-ACGU-3′.

Codon binding assays were performed as previously described (*19*). The 30S ribosomal subunits were prepared from *E. coli* MRE600 (*25*). To test that the mRNA fragments bound the 30S subunits, the mRNAs were 5′-end ^{32}P-labeled, titrated into 30S subunits, and monitored for binding using a filter binding assay (described below). ASLs were 5′-end ^{32}P-labeled using [γ-^{32}P]ATP (MP Biomedicals). Unlabeled ASLs over a range of concentrations (0−7.5 μM) were mixed with insignificant amounts, but radiochemically detectable (3000−5000 cpm), of 5′-end ^{32}P-labeled ASLs. A fixed ratio of unlabeled ASL to labeled ASL was maintained for each concentration in the range. The 30S ribosomal subunits (0.5 μM) were activated by incubation at 42 °C for 10 min and then slowly cooled to 37 °C. The subunits were then programmed with 50 μM mRNA for 15 min at 37 °C. The P-site was saturated with 1−2.5 μM tRNA^{fMet} (Sigma, St. Louis, MO) for 15 min at 37 °C before each concentration of ASL was added. A-Site binding was allowed to proceed for 30 min at 37 °C. The reaction mixtures were then placed on ice for 20 min and then filtered through nitrocellulose in a modified Whatman Schleicher and Schuell (Brentford, U.K.) 96-well filtration apparatus (*26*). Prior to filtration of experimental samples, the nitrocellulose filter was equilibrated in binding buffer at 4 °C for at least 20 min and each well of the filtration apparatus was washed with 100 μL of cold binding buffer [80 mM potassium cacodylate (pH 7.2), 20 mM $MgCl_2$, and 150 mM NH_4Cl]. Cold binding buffer (100 μL) was added to each sample, and the entire volume was quickly filtered. Each well was then washed at least twice with 100 μL of cold binding buffer. The nitrocellulose was dried out on paper towels, and the radioactivity was measured using a PhosphoImager (Molecular Dynamics, GE Healthcare). Data were measured for radioactive intensity using ImageQuant (Amersham) and were analyzed using single-site, nonlinear regression (Prism, GraphPad Software, Inc., San Diego, CA).

UV-Monitored Thermodynamic Experiments. The ASL samples were dissolved to obtain a concentration of 2 μM in 20 mM phosphate buffer. UV-monitored, thermal denaturations and renaturations were replicated four times and monitored by measuring UV absorbance (260 nm) using a Cary 3 spectrophotometer as previously described (*27*). The data points were averaged over 20 s and collected three times per minute with a temperature change of 1 °C/min from 4 to 90 °C. The data were analyzed (*28*), and the thermodynamic parameters were determined using Origin (Microcal).

NMR Spectroscopy. NMR spectrometers used for this study included the Bruker DRX500 and Varian Inova-600 instruments. NMR data were processed with either XWIN-NMR (Bruker Inc., Rheinstetten, Germany) or NMRPipe (*29*), and the analysis was conducted with SPARKY (*30*). For the samples dissolved in ^1H_2O, the WATERGATE (*31*) method was used to suppress the water signal. For samples dissolved in ^2H_2O, a low-power presaturation technique was used. NOESY (*32*) experiments of the samples in ^1H_2O were performed at low temperatures (2, 5, and 10 °C) to observe the exchangeable proton resonances. To aid the NMR resonance assignments of the nonexchangeable protons, the following experiments were performed: COSY, DQF-COSY (*42*), TOCSY (*33*), natural abundance ^{1}H−^{13}C HSQC, and ^{1}H−^{31}P HETCOR. For the determination of structures with the ASLs dissolved in ^2H_2O, NOESY experiments were conducted with different mixing times and at 22 °C. The NOESY spectra were recorded with mixing times of 50, 75, 100, 200, 300, and 400 ms, without removing the samples from the magnet. The spectra were acquired with spectral widths of 5000 Hz in both dimensions, 1024 points in t_2, 360 points with 64 scans per block in t_1, and a recycle delay of 1.5 s. The FIDs were processed with 60° phase-shifted sine bell apodization functions and third-degree polynomial baseline flattening in both dimensions. To improve the digital resolution for the cross-peak integration, the FIDs were zero-filled to 2048 × 2048 points.

Structure Determination. NMR spectra and the initial NMR-restrained molecular dynamics calculations of structure indicated that the 5 bp stems of the two ASLs adopted the A-form double-helix conformation. Therefore, the nucleotide base pairs were restrained by ensuring that their hydrogen bond donor−acceptor distances were canonical. To achieve planarity of the base pairs, a pseudoenergy term was applied. In addition to the NOE-derived restraints, the A-form backbone configuration was introduced by the use of proton−proton distances taken from an ideal A-form helix model previously generated using CNS (*34*). This addition increased the rate of convergence but did not affect the initial conformation of the stems or of the loops obtained with only the NMR-derived restraints that were used for the structure calculation. Thus, the effect of the complementary restraints on the stems did not propagate into the loops and, therefore, did not influence the loop conformations. The backbone and the ribose torsion angles were restrained to be within ±15° of the standard A-form values. NOESY mixing time studies also provided distance restraints between nonexchangeable protons in the loop region. The NOE cross-peaks were integrated by using the peak fitting Gaussian function and volume integration in SPARKY. The distance for each cross-peak was calculated and normalized to the nonoverlapped pyrimidine H5−H6 cross-peaks with a distance of 2.44 Å. Upper and lower bonds were assigned to ±20% of the calculated distances. The distances involving the unresolved protons, i.e., methyl of m^6A_{37} and methylene of cmo^5U_{34}, were assigned using pseudoatom notation to make use of the pseudoatom correction automatically computed by CNS.

High-resolution DQF-COSY spectra were used to characterize the sugar pucker based on the $^3J_{H1'-H2'}$ scalar couplings. Residues with nonobservable H1′−H2′ cross-peaks or with $^3J_{H1'-H2'}$ values of <3 Hz were restrained to the C3′-*endo* conformation, whereas in those with $^3J_{H1'-H2'}$ values appearing to be between 4 and 5 Hz, the ribose was left unconstrained to take into account the conformational averaging between the C3′-*endo* and C2′-*endo* conformations. The α and ζ torsion angles were restrained to exclude the *trans* conformation for those residues for which ^{31}P chemical shifts fell within the narrow range commonly seen for regular A-form RNA structures (*35*). The β, ϵ, and γ angles were

restrained on the basis of the $^{1}H-^{31}P$ HETCOR spectra as described previously (*35, 36*).

Structure calculations were performed using CNS and were based on published protocols (*37*) with minor modifications. Briefly, the initial structures consisted of extended strand conformations. The initial coordinates were regularized using simulated annealing and conjugate-gradient minimization to obtain good local geometry. Thus in the first stage, the regularized extended strands were subjected to 60 ps of torsion-angle molecular dynamics at 20000 K. The term w_{vdv} was set to 0.1 to ease rotational barrier crossing. The structures were then subjected to a slow-cooling torsion-angle molecular dynamics step where the temperature was reduced from 20000 to 1000 K over 60 ps. During this period, w_{vdv} was linearly increased from 0.1 to 1.0. In the third stage, the structures were slowly cooled from 1000 to 300 K over 6 ps by using Cartesian molecular dynamics. In the final stage, the structures were minimized by using the conjugate-gradient method. To obtain an ensemble of structures, this protocol was repeated with different initial velocities. The acceptance of the resulting structures was achieved by using the described criteria (*37*).

RESULTS

Modified nucleotides individually and in concert contribute to a tRNA's function in translation by providing new chemistries and structure (*9*). The anticodon stem and loop domain of $tRNA^{Val3}_{UAC}$, ASL^{Val3}_{UAC}, is modified at wobble position 34 and, 3′-adjacent to the anticodon, at the conserved purine 37 (Figure 1). To understand the important contributions of these modifications to the decoding function of *E. coli*'s $tRNA^{Val3}_{UAC}$, we analyzed and compared the properties of the unmodified ASL to that of the ASL modified with both cmo^5U_{34} and m^6A_{37} (Figure 1). Synthesis of ASL^{Val3}_{UAC}-cmo^5U_{34};m^6A_{37} required the development of a new strategy for protecting and later deprotecting the carboxylic acid function without producing the amide. The amide is readily formed from the commonly utilized ammonia or methylamine deprotection protocol. The presence and stoichiometric quantification of the modifications were confirmed through mass spectroscopy of the ASLs and HPLC of the composite mononucleosides and later by X-ray crystallography. The two ASL^{Val3} constructs were found to be unimolecular at concentrations for UV-monitored, thermal denaturations and NMR spectroscopy.

Modifications Order the Anticodon Loop. The chemistry and structure of ASL modifications alter the thermal stability of the RNA (*4, 27, 38, 39*). To determine and compare the thermodynamic and base stacking contributions of cmo^5U_{34} and m^6A_{37} to ASL^{Val3}_{UAC}, UV-monitored, thermal transitions and circular dichroism (CD) spectra of the unmodified and doubly modified ASLs were analyzed under conditions used for structure determination by NMR. The ASLs showed a cooperative behavior during the melting process by exhibiting one major transition (Figure 2). The melting temperatures (T_m) for the two ASLs were high due to the G-C rich stem region but were within error of each other. ASL^{Val3}_{UAC}-cmo^5U_{34};m^6A_{37} had a melting temperature of 71.8 ± 1.3 °C, whereas the T_m of unmodified ASL^{Val3}_{UAC} was 71.2 ± 1.1 °C (Table 1). cmo^5U_{34} is a free acid. However, the T_m of ASL^{Val3}_{UAC}-cmo^5U_{34};m^6A_{37} was not affected by the presence of Mg^{2+} at a concentration 5-fold greater than that of ASL, and neither was that of unmodified ASL. However, the modifications made a significant entropy contribution ($\Delta\Delta S$ = 25 cal K^{-1} mol^{-1}). This suggested an increase in the level of base stacking and order within the loop in the presence of modification and was confirmed by analyses of the degree of hyperchromicity for doubly modified ASL as compared to that of unmodified ASL. The hyperchromicity of ASL^{Val3}_{UAC}-cmo^5U_{34};m^6A_{37} was more than double that of unmodified ASL (Figure 2a and Table 1). Thus, it is inferred that the base stacking in the loop is enhanced by the modifications cmo^5U_{34} and m^6A_{37}.

The degree of ellipticity in the CD spectra of nucleic acids is most affected by the restricted rotation around the glycosidic bond, and base stacking interactions (*40*). Therefore, the contributions of modifications to base stacking and order can be ascertained by a comparison of CD spectra from the modified and unmodified ASLs (*40*). To further inves-

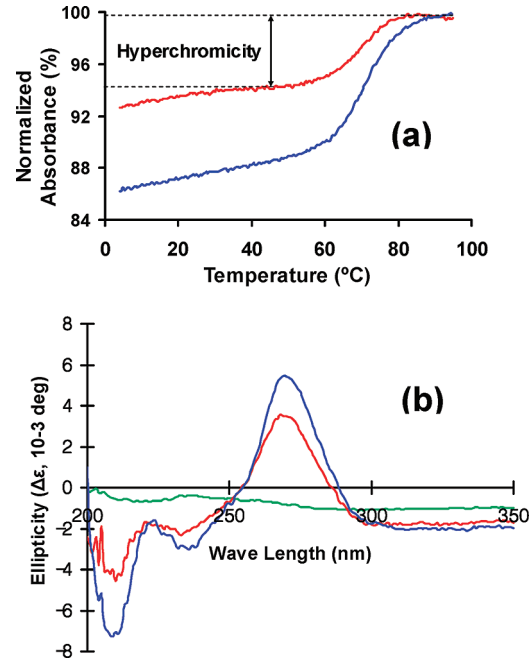

FIGURE 2: UV-monitored, thermal transitions and circular dichroism specta of unmodified and modified ASL^{Val3}_{UAC}. (a) Thermal transitions of modified and unmodified ASL^{Val3}_{UAC}. Unmodified ASL^{Val3}_{UAC} (red line) and ASL^{Val3}_{UAC} doubly modified with both cmo^5U_{34} and m^6A_{37} (blue line) were subjected to repeated thermal denaturations and renaturations monitored at 260 nm and under conditions identical to that for NMR analysis of structure. The melting temperatures for the ASLs were similar and high (~71.5 °C) due to the G-C rich stem region. This also demonstrated that the stems were very stable and, therefore, well-structured. The hyperchromicity measurements, denoted for unmodified ASL^{Val3}_{UAC}, differed considerably (Table 1). (b) Circular dichroism (CD) spectra of unmodified and modified ASL^{Val3}_{UAC}. CD spectra of unmodified ASL^{Val3}_{UAC} (red line) and ASL^{Val3}_{UAC}-cmo^5U_{34};m^6A_{37} (blue line) were collected under conditions identical to those used for structure determination by NMR. The introduction of modifications increased the intensity of the ellipticity at 260 nm: unmodified ASL^{Val3}_{UAC} < ASL^{Val3}_{UAC}-cmo^5U_{34};m^6A_{37}. The green line is that for buffer alone.

Table 1: Thermal Parameters of Unmodified and Modified ASL^{Val3}_{UAC}

ASL^{Val3}_{UAC}	T_m (°C)	ΔG (kcal/mol)	hyperchromicity (%)
unmodified	71.2 ± 1.1	−6.0 ± 0.4	5.0 ± 0.2
cmo^5U_{34};m^6A_{37}	71.8 ± 1.3	−5.3 ± 0.3	11.0 ± 0.2

tigate the effect of modifications on the secondary structure of the loop, CD spectra of the two ASL^{Val3}_{UAC} forms were collected under the same buffer conditions that were used for thermal denaturations and NMR structure determination. The resulting spectra (Figure 2b) exhibited the three expected ellipticities for an RNA hairpin at 210, 230, and 260 nm. The negative and positive ellipticities at 210 and 260 nm, respectively, were characteristic of right-handed helices (*40*). The third ellipticity at 230 nm could be attributed to the anticodon loop. However, it is the ellipticity at 260 nm that most accurately reflects differences in base stacking (*41*). The introduction of modifications significantly increased the intensity of the ellipticity at 260 nm (Figure 2). While the thermal transitions observed in UV-monitored thermal denaturations are biased toward base stacking interruptions in stems, CD spectra monitor stems and loops more equally. Thus, our CD results indicate that the base stacking interactions in the ASLs, more precisely in the loops, were enhanced by the presence of cmo^5U_{34} and m^6A_{37}. The increased ellipticity, together with the enhanced hyperchromicity observed during the UV-monitored melting experiments, supports the conclusion that the modifications within the ASL loop increase the level of base stacking.

Recognition of Valine Codons at the Ribosomal A-Site. $tRNA^{Val}_{UAC}$ decodes GUA and wobbles to GUG but also decodes GUU and GUC (*14*). The cmo^5U_{34}-U3 and cmo^5U_{34}-C3 base pairs were unexpected in light of the wobble hypothesis. However, isoaccepting species of Ala and Pro tRNAs with cmo^5U_{34} also have been shown to read their respective codons ending in U and C (*18, 42, 43*). Recent studies of mutant strains of *Salmonella enterica* have shown that mutants consisting of only the cmo^5U_{34}-containing $tRNA^{Val}$ isoacceptor and, thus, lacking the other $tRNA^{Val}$ isoacceptor were viable (*44*). Furthermore, cmo^5U_{34} is required for effective reading of Val, Pro, and Ala codons ending with G (*44*). In an effort to determine the contributions of cmo^5U_{34} and m^6A_{37} in the tRNA's binding of the four codons, unmodified ASL^{Val3}_{UAC} and fully modified ASL^{Val3}_{UAC}-cmo^5U_{34};m^6A_{37} were assayed for binding affinities for each of the four valine codons in the A-site of the 30S ribosomal subunit. The 30S subunit was programmed with a message consisting of the initiation codon (AUG) at the P-site and one of the valine codons at the A-site. Binding of the ASL to codons in the A-site of the 30S ribosomal subunit is comparable to binding of tRNA to codons on the 70S ribosome (*45*). To ensure binding of ASL^{Val3}_{UAC} to the A-site only, the P-site was saturated with *E. coli* $tRNA^{fMet}$. ASL^{Val3}_{UAC} and ASL^{Val3}_{UAC}-cmo^5U_{34};m^6A_{37} bound the cognate codon GUA with submicromolar K_d values of 0.37 ± 0.06 and 0.17 ± 0.03 μM, respectively (Figure 3 and Table 2). ASL^{Val3}_{UAC} did not bind to GUG, in comparison to its fully modified counterpart, ASL^{Val3}_{UAC}-cmo^5U_{34};m^6A_{37}. ASL^{Val3}_{UAC}-cmo^5U_{34};m^6A_{37} bound GUG with an affinity of 1.96 ± 0.32 μM (Table 2). These results are consistent with those of the growth experiments in vivo (*44*). Only the fully modified ASL^{Val3}_{UAC}-cmo^5U_{34};m^6A_{37} was found to bind GUU and did so with a K_d of 1.93 ± 0.70 μM. We had succeeded in determining the X-ray crystallographic structure of ASL^{Val3}_{UAC}-cmo^5U_{34};m^6A_{37} bound to GUC, as well as the other three valine codons (*46*). Therefore, ASL^{Val3}_{UAC}-cmo^5U_{34};m^6A_{37} will bind to GUC, but we could not determine a binding constant under our experimental conditions or using ribosome binding conditions of other investigators (*23, 43*). The cmo^5U_{34}-containing $tRNA^{Val3}_{UAC}$, in the absence of other $tRNA^{Val}$ isoacceptors, was able to read all four valine codons in vivo, although the extent of growth of cells was reduced (*44*). The reduction in the extent of growth was attributed mostly to the inefficiency of the cmo^5U_{34}-modified $tRNA^{Val3}_{UAC}$, in comparison to isoacceptor $tRNA^{Val}_{GAC}$, in reading the GUC codon (*44*). The GUC codon tends to be read by the $tRNA^{Val}_{GAC}$ isoacceptor. Therefore, our inability to detect the binding of ASL^{Val3}_{UAC}-cmo^5U_{34};m^6A_{37} to GUC may be due to the reduced efficiency of the UAC anticodon in base pairing with the GUC codon, even with the cmo^5U_{34} modification present (*44*). Under experimental conditions different from those reported here, the $tRNA^{Ala}_{UGC}$ species with cmo^5U_{34} was observed to bind weakly to GCC (*43*).

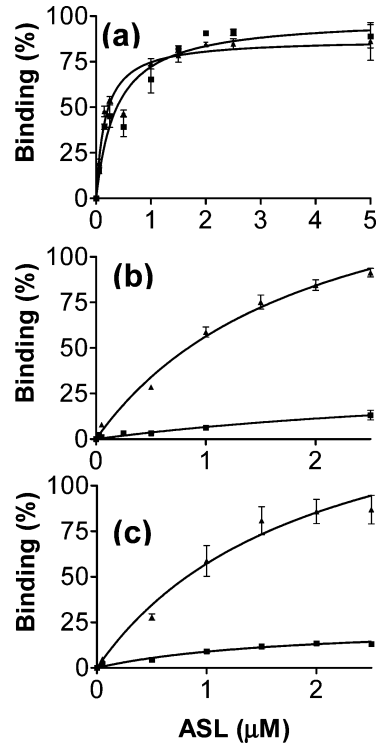

FIGURE 3: Binding of unmodified and modified ASL^{Val3}_{UAC} to valine codons at the A-site of *E. coli* 30S ribosomal subunits. Codons in the A-site of the 30S subunit were titrated with increasing concentrations of radiochemically, 5′-end ^{32}P-labeled ASLs (0−7.5 μM). The 30S subunits (0.5 μM) were programmed with mRNA (50 μM) and saturated with *E. coli* $tRNA^{fMet}$ (1−2.5 μM). The binding curves were analyzed with single-site, nonlinear regression and the dissociation constants (K_d) calculated (see Table 2). (a) Binding to the GUA codon: unmodified ASL^{Val3}_{UAC} (■) and ASL^{Val3}_{UAC}-cmo^5U_{34};m^6A_{37} (▲). (b) Binding to the GUG codon: unmodified ASL^{Val3}_{UAC} (■) and ASL^{Val3}_{UAC}-cmo^5U_{34};m^6A_{37} (▲). Only ASL^{Val3}_{UAC}-cmo^5U_{34};m^6A_{37} was found to bind the GUG codon. (c) Binding to the GUU codon: unmodified ASL^{Val3}_{UAC} (■) and ASL^{Val3}_{UAC}-cmo^5U_{34};m^6A_{37}. Only ASL^{Val3}_{UAC}-cmo^5U_{34};m^6A_{37} was found to bind the GUU codon (▲).

Table 2: Affinity of Unmodified and Modified ASL^{Val3}_{UAC} for the Valine Codons

A-site codon	K_d (μM) for unmodified ASL^{Val3}_{UAC}	K_d (μM) for ASL^{Val3}_{UAC} cmo^5U_{34};m^6A_{37}
GUU	>2000	1.93 ± 0.70
GUC	>2000	>2000
GUA	0.37 ± 0.06	0.17 ± 0.03
GUG	>2000	1.96 ± 0.32

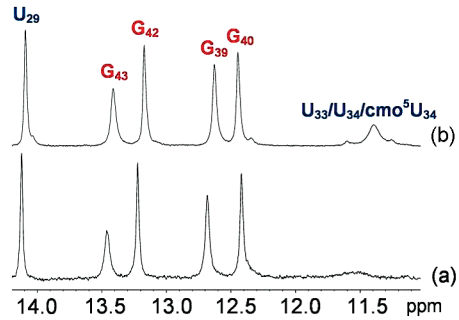

FIGURE 4: Detection of the base-paired imino protons of the ASLs by NMR. The base-paired, imino proton region of the 1D ^{1}H NMR spectra of unmodified and modified ASL$^{Val3}_{UAC}$ exhibited five low-field-shifted resonances between 12.00 and 14.50 ppm: (a) ASL$^{Val3}_{UAC}$ and (b) ASL$^{Val3}_{UAC}$-cmo^{5}U$_{34}$;m^{6}A$_{37}$. The chemical shift dispersion observed in this region is characteristic of imino protons engaged in Watson−Crick base pairing. As expected, the number of peaks identified in this region corresponded exactly to the number of base pairs present in the stem of the four ASLs. The imino proton resonance of U$_{34}$ is more resolved in the spectrum of ASL$^{Val3}_{UAC}$-cmo^{5}U$_{34}$;m^{6}A$_{37}$, indicating that on the NMR time scale the rate of exchange with the solvent is decreased and suggesting that the decreased exchange rate is induced by an increase in the level of base stacking.

Resonance Assignments. UV-monitored thermal transitions and the CD spectra indicated that the cmo^{5}U$_{34}$ and m^{6}A$_{37}$ modifications contributed to the ordered structure of ASL$^{Val3}_{UAC}$. With the purpose of understanding the degree to which the modifications influence anticodon conformation and dynamics, we determined the solution structures of the unmodified and fully modified ASL$^{Val3}_{UAC}$. A series of one- and two-dimensional NMR spectra were collected. The exchangeable, base-paired, imino proton resonances were identified and assigned using one-dimensional (1D) and Watergate-NOESY spectra. The nonexchangeable proton signals were identified and assigned using a combination of one-dimensional, COSY, DQF-COSY, ^{1}H−^{31}P HETCOR, natural abundance ^{1}H−^{13}C HSQC, and NOESY spectra, following well-established procedures (*35, 47*). The addition of 5 mM Mg^{2+} did not alter the NMR spectra, and higher concentrations of Mg^{2+} will broaden the NMR resonances, reducing the spectral resolution (*4*). Therefore, the NMR spectra were collected without Mg^{2+} being added to the ASLs.

Assignment of Exchangeable Proton Resonances. The base-paired, imino proton region of the 1D spectra exhibited five low-field-shifted resonances between 12.00 and 14.50 ppm for each of the ASLs (Figure 4). The chemical shift dispersion observed in this region was characteristic of imino protons engaged in Watson−Crick base pairing (*35, 47*). The number of base paired imino proton peaks corresponded exactly to the number of base pairs present in the stem of the four ASLs, indicating that the stems of the ASLs adopted stable duplex secondary structures. As a result, we initially assigned sequential resonances from the NOESY spectra by assuming that the stem conformations were close to that of the right-handed, A-form RNA duplexes. Later, this was to be confirmed by the "NOE walk" of spectra in D$_2$O (*32*). The spectra of ASL$^{Val3}_{UAC}$-cmo^{5}U$_{34}$;m^{6}A$_{37}$ exhibited two minor imino proton resonances. These small signals could be due to heterogeneity of conformation, or to the presence of failed sequences (impurities) that occurred during synthesis that could not be removed during the different steps of the oligonucleotide purifications. Also, two broad resonances were identified between the chemical shifts of 11.60 and 11.30 ppm in the spectra of modified ASL. In contrast, the same peaks were poorly resolved, as one very broad resonance, in the spectrum of unmodified ASL$^{Val3}_{UAC}$. These resonances were attributed to the non-hydrogen-bonded, imino protons of the U$_{33}$ and cmo^{5}U$_{34}$ residues that are located in the loop. Thus, U$_{33}$ and cmo^{5}U$_{34}$ exhibit a slower than expected exchange with the solvent in comparison to unmodified U$_{34}$. The slower exchange could be attributed to a change in their pK_a values or to an ordering of the loop through base stacking. In fact, the pK_a values of the hydrogens at the N3 position of U (HN3), mcm^{5}U, and cmnm^{5}U have been determined to be 9.38, 8.20, and 8.44, respectively (*48–50*). The pK_a of HN3 of cmo^{5}U has been estimated to be ~8.02 (*51*). Though modification of position 5 of uridine reduces the pK_a, it is still significantly higher than the pH of the NMR experiments (pH 6.2) and the physiological pH. If the modifications contribute to the base stacking, then one would expect that HN3 of unmodified U$_{34}$ within ASL$^{Val3}_{UAC}$-m^{6}A$_{37}$, a homologue of ASL$^{Val3}_{UAC}$ containing only the m^{6}A$_{37}$ modification, may exchange at a rate slower than that of completely unmodified ASL$^{Val3}_{UAC}$. In a recently recorded NMR spectrum of ASL$^{Val3}_{UAC}$-m^{6}A$_{37}$, the proton of N3 of U$_{34}$ was found to be in a slower exchange than that of unmodified ASL (F. A. P. Vendeix et al., personal communication). Thus, the more resolved resonances of the uridine imino protons in the spectra of ASL$^{Val3}_{UAC}$-cmo^{5}U$_{34}$;m^{6}A$_{37}$ suggest that in the presence of modifications the imino protons of U$_{33}$ and cmo^{5}U$_{34}$ were protected from rapid exchange with the solvent. These results are consistent with an increased order through base stacking in the anticodon loop.

The resonance most shifted to the low field at 14.09 ppm and observed in the NOESY spectra of the ASLs was readily assigned to U$_{29}$ since only one uridine was present in the stem sequence (Figure 4). This cross-peak was a convenient starting point for the specific sequential resonance assignments of the imino−imino and imino−amino proton connectivities. Nevertheless, the resonance observed at 13.42 ppm on the 1D spectra of the ASLs could not be identified on the NOESY spectra, indicating fast exchange between the imino proton and the protons of water. The fast exchange could be explained by the fraying of the terminal stem base pair (C$_{27}$-G$_{43}$), and therefore, this resonance was assigned to the G$_{43}$ imino proton. Analogues of unmodified ASL$^{Val3}_{UAC}$ were synthesized with the reverse orientation of the C$_{28}$-G$_{42}$ and U$_{29}$-A$_{41}$ base pairs. NMR analysis of these analogues' spectra clarified the imino signal assignments and helped in the assignment of the many guanosine spin systems.

Assignment of Nonexchangeable Proton Resonances. The methylene group of cmo^{5}U$_{34}$ and the methyl group of m^{6}A$_{37}$ were identified and assigned on the basis of their distinctive high-field, sharp resonances observed in the 1D spectra. The pyrimidine H5 and H6 resonances were readily identified on the COSY and ^{1}H−^{13}C HSQC spectra. In the case of unmodified ASL$^{Val3}_{UAC}$, nine cross-peaks corresponding to the total number of Cs and Us present in the sequence were observed. This was not the case for ASL$^{Val3}_{UAC}$-cmo^{5}U$_{34}$;m^{6}A$_{37}$, where only eight cross-peaks were present (Figure 5). The missing cross-peak confirmed that the H5 proton of U$_{34}$ was substituted by the functional group cmo^5

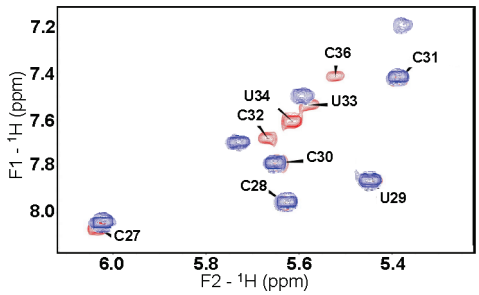

FIGURE 5: Superimposed $^{1}H-^{1}H$ COSY spectra of unmodified and modified ASL^{Val3}_{UAC}. Spectra were collected under identical conditions for ASL^{Val3}_{UAC} (red) and ASL^{Val3}_{UAC}-cmo^5U_{34};m^6A_{37} (blue) (^2H_2O, 500 MHz). The spectral region corresponding to the through-bond correlation between the pyrimidine H5 and H6 protons demonstrates significant homologies, with the notable exceptions of U_{34} for ASL^{Val3}_{UAC}-cmo^5U_{34};m^6A_{37}. Each peak is labeled with its corresponding residue where the H5−H6 correlation is observed.

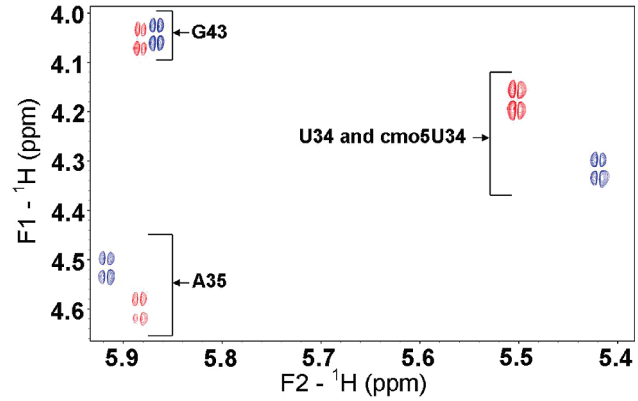

FIGURE 6: Determination of ribose conformation from the ^{1}H DQF-COSY spectra. The H2′−H1′ regions of DQF-COSY spectra of ASL^{Val3}_{UAC} (red) and ASL^{Val3}_{UAC}-cmo^5U_{34};m^6A_{37} (blue) are superimposed and were used to assess the sugar pucker of the individual nucleotides. The C2′-*endo* conformation is adopted by residues G_{43}, A_{35}, and U_{34}/cmo^5U_{34}.

and also allowed us to unambiguously assign the H5 and H6 protons of U_{34}.

The H1′, H6, H8, and H2 protons were assigned by using the NOESY spectra on which the H1′−H6/H8 NOE sequential connectivity could be followed from the 5′- to 3′-end of the ASLs (Supporting Information). Breaks in the sequence between the connectivity of U_{33} H1′−U_{34} H6 and that of C_{36} H1′−A_{37} H8 were observed on the spectra of two ASLs. ASL^{Val3}_{UAC} exhibited a missing NOE cross-peak between A_{37} H8 and A_{38} H1′. An additional resonance was assigned to an NOE between A_{35} H8 and U_{33} H1′. With the introduction of cmo^5U_{34} and m^6A_{37}, we observed that the H1′ protons of specific loop residues experience changes in chemical shift. The H1′ protons of U_{34}, A_{35}, C_{36}, and A_{37} had altered chemical shifts in the F2 dimension (Supporting Information). In addition, these spectra indicated that even the unmodified ASL^{Val3}_{UAC} had at least one U_{33} connectivity that is routinely associated with the canonical U-turn motif of tRNA anticodons, the U_{33} H1′−A_{35} H8 NOE.

The DQF-COSY and COSY spectra of the ASLs revealed that most of the nucleotides were completely within the expected C3′-*endo* conformation. However, just three of the ribose moieties, those of G_{43}, A_{35}, and U_{34}/cmo^5U_{34} having $^{3}J_{H1'-H2'}$ couplings between 3 and 5 Hz, exhibited almost equally proportioned C3′-*endo* and C2′-*endo* conformations (Figure 6) (*35*). This suggested that the conformational dynamics of the sugar pucker was not affected by the modifications. Since the ribose conformations were established for the 17 nucleotides, the identification of the H2′ resonances could be confirmed through observation of the strong cross-peaks to the H1′ protons in the short mixing time NOESY experiment (*35*). The H3′ protons were identified by using the $^{1}H-^{31}P$, HETCOR, and $^{1}H-^{13}C$ HSQC experiments. A nearly complete identification of each individual nucleotide's proton resonances was accomplished by using the sequential connectivities of the H1′−H8/H6, H2−H8, and H3′−H8 NOE cross-peaks to assign the H1′, H2′, and H3′ protons. The remaining anomeric protons (H4′ and H5′/H5″) were identified on the $^{1}H-^{13}C$ HSQC spectra due to their distinctive ^{13}C chemical shift dispersion. The H4′ protons were assigned by using the H1′−H4′ NOE cross-peaks observed with long mixing time. Due to severe resonance overlaps, only a partial assignment of the H4′ and H5′/H5″ protons was achieved.

The phosphorus chemical shifts observed in the $^{1}H-^{31}P$ HETCOR spectra of the ASLs were between 0.2 and 2.6 ppm (Supporting Information). A group of cross-peaks that corresponded to the loop and the stem residues was found between 0.2 and 1.5 ppm. The U_{33}H3′−P_{34} cross-peak of all of the ASLs exhibited a ∼1 ppm downfield shift of the phosphorus compared to the rest of the residues which exhibited moderate chemical shift changes ($\Delta\delta = 0.1-0.2$ ppm). This cross-peak resonated within the chemical shift window common to regular A-form structures. However, the downfield shift was more pronounced for ASL^{Val3}_{UAC}-cmo^5U_{34};m^6A_{37} ($\Delta\delta = 0.4-0.5$ ppm) than for unmodified ASL^{Val3}_{UAC} ($\Delta\delta = 0.2$ ppm).

The spectral analyses described above and assignments lead to several conclusions. The high quality of the different spectra indicated well-behaved unmodified and modified ASLs under the NMR experimental conditions. The A-RNA-type conformation adopted by the two stems was confirmed by the NOE connectivities. Although slight differences in NOE patterns and chemical shifts were found between the ASLs, the stability and the similarity of their respective stems were emphasized by the considerable identity of the resonances assigned to the residues of the stems. In comparison with unmodified ASL^{Val3}_{UAC}, the insertion of modified bases in the loop induced noticeable changes in chemical shifts which indicated specific structural variations. The NMR results confirmed the correlation between the modification of the ASL loop and the enhanced base stacking as observed in the increased ellipticity of the CD spectrum and the hyperchromicity of the UV-monitored thermal denaturations. In addition, the interruption in the NOE sequential connectivity between U_{33} H1′ and U_{34} H6, the NOE cross-peak connecting A_{35} H8 to U_{33} H1′, and the low-field-shifted U_{33} H3′−P_{34} cross-peak were among the distinctive NMR "fingerprint" resonances that indicate a canonical "U" turn in anticodon domains (*52*).

Structure Determination. Distance and Angle Restraints. The distance and dihedral angle restraints required for structure determination were derived from NOESY cross-peaks and *J* couplings (DQF-COSY and ^{31}P HETCOR spectra). The data obtained from the UV-monitored thermal transitions, the CD spectra, and the NMR experiments clearly

indicated an A-form helix conformation adopted by the stems of the ASLs studied herein. These data also showed that the modifications in the anticodon loop did not induce a conformational change or dynamics in the stem. On the basis of the observations described above, and knowing that posttranscriptional modifications do not alter the overall helical structure of $tRNA^{Val}$ (*53*), we focused on elucidating the structural differences located in the loops. Therefore, the NMR torsion-angle and distance restraints from the two stems were complemented with distance restraints that yield the conventional A-form helix conformation, as reported and utilized by others (*52*). The restraints that were added to the stems of modified and unmodified ASLs did not alter the structures of the loops but did enhance the rate of convergence (from 40 to 60%) during structure calculations. In the loop region alone, a total of 76 and 90 NOE-derived distance restraints were obtained for unmodified ASL^{Val3}_{UAC} and ASL^{Val3}_{UAC}-cmo^5U_{34};m^6A_{37}, respectively. (See the structure deposition entries for detailed structure determination statistics.)

We and others have explored the possibility of noncanonical hydrogen bonding across the ASL loop between loop residues C_{32} and A_{38} (*4, 9, 54*). However, the hydrogen involved has yet to be observed by NMR spectral analyses. Still, the distance between A_{38} N6 and C_{32} O2 in the two ASL^{Val3}_{UAC} structures was determined to be ~2.68 Å, and this is strongly suggestive of noncanonical hydrogen bonding between A_{38} and C_{32} occurring at the base of the stem. Protonation of N1 of A_{38} would facilitate formation of such a base pair and does not require a significant reduction in pH. The protonation of N1 of A_{38} has been observed in the structure determination of other ASLs under the solution conditions in which the pH was only moderately acidic (pH 5.5−7.0) (*5, 54*).

The α and ζ dihedral angles were estimated from the ^{31}P chemical shift values and were restrained to exclude the *trans* conformation (*35*) with the exception of the $U_{33}-P-U_{34}$ angle, which was left unrestrained. The β angles were estimated from the $^3J_{P-H5'}$ and $^3J_{P-H5''}$ scalar couplings (*47*). The absence of intense cross-peaks between the phosphorus atoms and the H5′/H5″ protons in the $^1H-^{31}P$ HETCOR spectra indicated that the β angles were in the *trans* conformation commonly observed in A-form RNA. The γ angles were restrained to adopt the *trans* conformation for residues having a weak P−H4′ cross-peak. Otherwise, the γ angles were left unconstrained. Since all $^3J_{P-H3'}$ coupling constants were determined to be greater than 5 Hz, the dihedral ϵ angles were restrained to exclude the *gauche*$^-$ (g^-) conformation for all residues in the loop.

The glycosidic torsion angle χ was restrained to the *anti* conformation as dictated by the weak intensity of the cross-peak observed between H1′ and H6/H8 for all loop residues. The ribose pucker of each residue was restrained on the basis of the $^3J_{H1'-H2'}$ scalar couplings. Thus, the ribose puckers of G_{43}, unmodified U_{34}, cmo^5U_{34} and A_{35} were left unconstrained to take into account the conformational averaging between the C3′-*endo* and C2′-*endo* conformations.

Description of the ASL Loops. After collection of the distances and dihedral angles derived from NOE and *J* coupling constants, respectively, the solution structures of the four ASLs were determined by torsion-angle molecular dynamics simulation (*37*). Twenty-five structures were generated for each ASL, each of which contained no violations of NOE restraints greater than 0.5 Å and no dihedral angle violations greater than 5°. In addition to these selection criteria, a structure was rejected if the root-mean-square deviation (rmsd) of bonds varied from ideal values by greater than 0.02 Å or the rmsd of angles was greater than 2.0°. Among the 25 structures that converged, 10 had low total energy and no restraint violations. These 10 lowest-energy structures were in agreement with the NMR data and were selected to represent the final ensemble.

We observed interesting similarities and important distinctions between unmodified ASL^{Val3}_{UAC} and ASL^{Val3}_{UAC}-cmo^5U_{34};m^6A_{37} structures. The ASL stems were identical due to the A-form RNA structure imposed by the many NMR-derived restraints, and those few added restraints that were consistent with an RNA duplex. Structures of the unmodified and fully modified ASL^{Val3}_{UAC} (Figure 7) featured α-helical axes of the loops that were not aligned with the respective stems. In addition, the seven nucleotides of the loop exhibited helical conformations stacked to different degrees from the 5′- to 3′-end of the loop, as previously confirmed by the sequential NOE cross-peak connectivity.

In contrast to the stems, there were distinctive differences between anticodon loops. The anticodon loop of ASL^{Val3}_{UAC} was less structured than that of ASL^{Val3}_{UAC}-cmo^5U_{34};m^6A_{37} (Figure 7). The rmsd values for each of the loop nucleotides of ASL^{Val3}_{UAC}-cmo^5U_{34};m^6A_{37} were consistently lower than those of the unmodified ASL (Figure 7c). The unmodified U_{34} was the most dynamic of the loop residues. cmo^5U_{34} appears to be as dynamic as that of the unmodified U_{34} (Figure 7c). However, the methylene protons of cmo^5U_{34} had sequential NOE cross-peaks to A_{35} H8 and an intraresidue NOE to its H6 and H1′ protons. We suspect that the free rotation around the carbon of the methylene group of the cmo^5U_{34} residue produced different orientations that are responsible for the higher rmsd, even though the base and 5-oxy group were fixed by NOE restraints. The N^6-methyl of A_{37} exhibited NOE cross-peaks to A_{38} H1′ and H2, yet the methyl group of m^6A_{37} was observed to have two distinct orientations. The orientation of the methyl group toward the plane defined by the aromatic ring of A_{38} was observed in 7 of 10 structures (Figure 7). The three structures with the methyl group oriented away from the plane of A_{38} exhibited a higher rmsd for cmo^5U_{34} (Figure 8a,c). Stereochemical hindrance of the methyl group constrained the m^6A_{37} nucleotide to a position translated outward from the loop (~1.6 Å) relative to that of A_{37} of the unmodified ASL^{Val3}_{UAC} (Figure 8). As a consequence, the loop of ASL^{Val3}_{UAC}-cmo^5U_{34};m^6A_{37} is broader than that of unmodified ASL^{Val3}_{UAC} (Figures 8 and 9). With the exception of cmo^5U_{34}, the rmsd values for each of the loop nucleotides of the seven aforementioned structures of ASL^{Val3}_{UAC}-cmo^5U_{34};m^6A_{37} were consistently lower than those of the unmodified ASL (Figure 7c). This indicated that the anticodon loop of ASL^{Val3}_{UAC}-cmo^5U_{34};m^6A_{37} was more highly ordered than that of ASL^{Val3}_{UAC}. Thus, the loops of the modified ASL exhibited restricted dynamics caused by a steric hindrance to the positioning of the N^6-methyl of A_{37} and to the geometry of the cmo^5 moiety due to hydrogen bonding by the base and that of the 5-oxy group (Figures 8 and 9). The differences in loop architecture and dynamics were supported by the numbers of restraints for the loop nucleotides. The NMR-

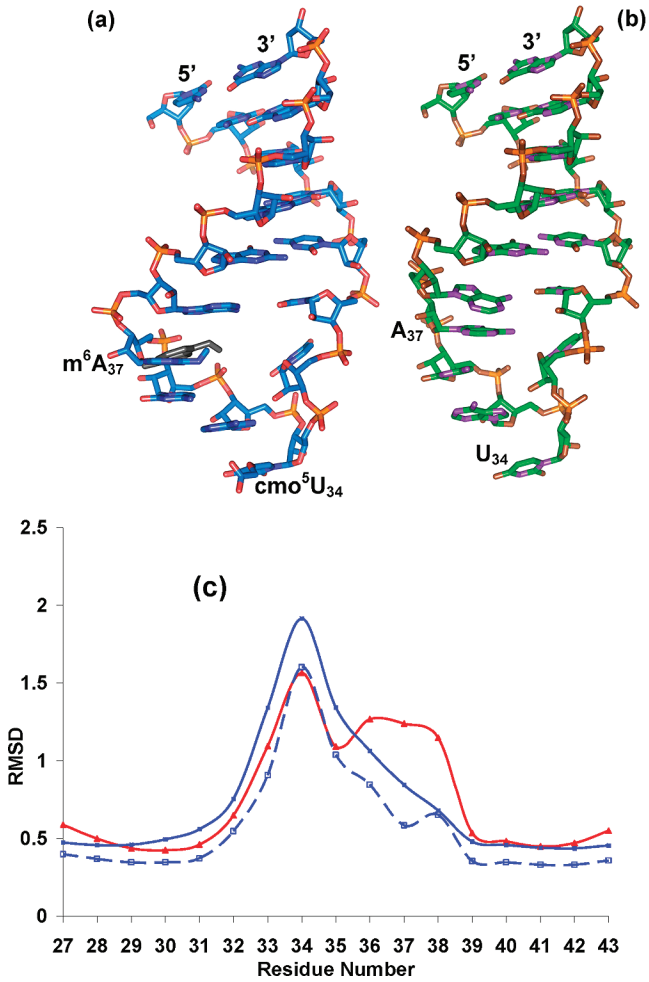

FIGURE 7: Solution structures of ASL^{Val3}_{UAC}-cmo^5U_{34};m^6A_{37} and ASL^{Val3}_{UAC} and the rmsd for each of their nucleotides. Families of structures were derived from torsion-angle-restrained, molecular dynamics calculations and then averaged to yield the structures of (a) ASL^{Val3}_{UAC}-cmo^5U_{34};m^6A_{37} and (b) ASL^{Val3}_{UAC} with no violations. The modified residues (cmo^5U_{34} and m^6A_{37}) of ASL^{Val3}_{UAC}-cmo^5U_{34};m^6A_{37} are labeled. The alternate position of the m^6A_{37} is depicted with the nucleotide colored dark gray. (c) Individual nucleotide average rmsd for unmodified ASL^{Val3}_{UAC} (red) and ASL^{Val3}_{UAC}-cmo^5U_{34};m^6A_{37} (blue). The rmsds of all heavy atoms (angstroms) from the mean are plotted for each of the nucleotides of the two ASLs. The blue dashed curve corresponds to the rmsd of seven ASL^{Val3}_{UAC}-cmo^5U_{34};m^6A_{37} structures in which one orientation of the methyl group of m^6A_{37} is taken into account, above the plane of A_{37}.

based molecular dynamics simulations were conducted with an average of 16 restraints per loop residue for the two ASLs. Thus, the differences were due to the NOE cross-peaks generated by the methyl and the methylene groups of m^6A_{37} and cmo^5U_{34}, respectively. However, more dependable information about the distinguishing dynamics of these loops could be obtained from a detailed study of relaxation measurements using stable samples isotopically labeled with ^{13}C and ^{15}N.

Although the DQF-COSY spectrum of the unmodified ASL^{Val3}_{UAC} indicated that some loop nucleotides were in a C3′-*endo*−C2′-*endo* sugar equilibrium, the furanose rings were found to adopt preferentially the C3′-*endo* conformation. A_{35} of the doubly modified ASL exhibited a C2′-*endo* sugar conformation. The χ angles of m^6A_{37} and cmo^5U_{34} were confirmed to be in the *anti* conformation. However, analysis of the unmodified ASL family of structures revealed that

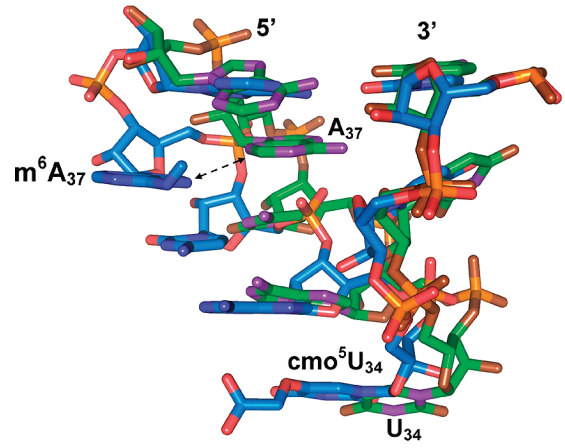

FIGURE 8: Superimposition of the average structures of the loop residues of ASL^{Val3}_{UAC}-cmo^5U_{34};m^6A_{37} with that of ASL^{Val3}_{UAC}. The seven nucleotides of the loop differ in the degree of stacked helical conformation and base orientation from the 5′- to 3′-end of the loops. The stereochemical hindrance of the methyl group constrained the m^6A_{37} nucleotide to a position translated outward from the loop (~1.6 Å) relative to that of A_{37} of the unmodified ASL^{Val3}_{UAC} (see the dashed arrow).

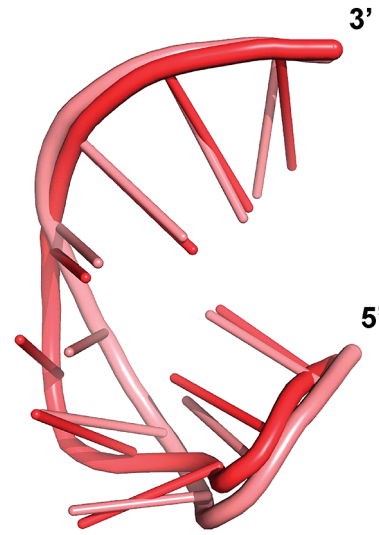

FIGURE 9: Loop structure of ASL^{Val3}_{UAC}-cmo^5U_{34};m^6A_{37} in solution compared to that of the crystallographic structure on the ribosome. The restrained molecular dynamics structure of ASL^{Val3}_{UAC}-cmo^5U_{34};m^6A_{37} in solution (red) is superimposed upon the X-ray crystallographic structure (pink). ASL residues C_{32}−G_{40} are shown. The crystal structures of the ASL bound to codon GUA and the other three valine codons were determined at a resolution of 2.8 Å.

the χ angle of U_{34} was mostly *syn* but oscillated between the *syn* and *anti* conformations.

The folding of the ASLs is marked by a turn of the backbone between the invariant U_{33} and the wobble position U_{34}. This folding is allowed by the high degree of rotation of the angle α. The P−O5′ torsion angle of residue 34 (of the two ASLs) was in the *gauche*$^+$ (g^+ or $^+$sc) conformation instead of the g^- orientation commonly found in the helical conformation. These turns are generally defined as π-turns (*48*) and are typically found at the invariant U_{33} of tRNAs, where the predominant form exhibited is the "U-turn". They are also known for stabilizing and ordering the anticodon loop by base−phosphate stacking interaction and hydrogen bonding. Thus, the 5′-phosphate attached to O3′ of residue U_{34} is engaged to some extent in stacking interactions with U_{33}. The hydrogen bond between U_{33} O2′ and A_{35} N7 is

characteristic of U-turns (*52*) and was observed in the loop of the two ASLs. This bond was found to be shorter (2.85 Å) in the case of ASL^{Val3}_{UAC}-cmo^5U_{34};m^6A_{37}. Hydrogen bonds between U_{33} H3 and C_{36} PO_2 and between A_{35} N6 and U_{33} O2′ were not observed.

DISCUSSION

The six prokaryotic and eukaryotic tRNA species for alanine, leucine, proline, serine, threonine, and valine that have the posttranscriptional oxy modification of wobble position uridine 34 (xo^5U_{34}) (*4*) are able to read fully 18−24 of the 61 amino acid codons (*9*). Previously, we found that modifications at wobble position U_{34} are directly correlated to the need of certain tRNAs to discriminate at the third position of the codon (*6*). The lysine and asparagine codons are each 2-fold degenerate and share a codon box. Therefore, the codons for lysine and asparagine differ only in the third position. We have shown that modifications at positions 34 and 37 of ASL^{Lys}_{UUU} (ASL^{Lys}_{UUU}-s^2U_{34};t^6A_{37}) are required for the recognition of both lysine codons, even the cognate AAA (*6*). Valine codes, however, are 4-fold degenerate and are translated by tRNAs that do not discriminate among the third base of the codon. We have shown here that modifications are not required for ASL^{Val3}_{UAC} to bind the cognate codon GUA. However, the cmo^5U_{34} and m^6A_{37} modifications are necessary for the ASL to bind GUG and GUU. In addition, the fully modified ASL^{Val3}_{UAC}-cmo^5U_{34};m^6A_{37} binds GUC, for we have determined the structure in the A-site of the small subunit of the ribosome (*46*). Unfortunately, we were not able to determine a binding constant. However, the cmo^5U_{34}-modified $tRNA^{Ala}_{UGC}$ was shown to bind weakly to GCC (*43*). In the binding of GCC by $tRNA^{Ala}_{UGC}$, the first and second base pairs are C_{36}-G1 and G_{35}-C2, respectively, whereas in the binding of GUC by ASL^{Val3}_{UAC}-cmo^5U_{34};m^6A_{37}, the first and second base pairs are C_{35}-G1 and A_{36}-U2, respectively. The stronger base pairing and stacking of the two G-C pairs formed when $tRNA^{Ala}_{UGC}$ binds GCC may facilitate the cmo^5U_{34}-C pairing at the third position. Furthermore, studies *in vivo* have shown that the cmo^5U_{34}-modified $tRNA^{Val3}_{UAC}$ recognizes the GUC codon, although poorly (*44*).

An understanding of the physicochemical contributions of cmo^5U_{34} to anticodon structure and dynamics in solution, and on the ribosome, will provide critical insights into the role of modifications in reading of the universal codes. The results obtained from the UV-monitored thermal transition, the degree of ellipticity observed in the CD spectra, and the NOE connectivities of NMR spectra allowed us to confirm that the secondary structure of the stems of the unmodified and modified *E. coli* ASL^{Val3}_{UAC} adopted the A-RNA conformation. Moreover, these studies demonstrated that the insertion of modified bases at positions 34 (wobble position) and 37 did not induce any conformational changes in the stem. However, significant differences in anticodon loop conformations between unmodified and modified ASLs were revealed by the variations in UV hyperchromicity, CD ellipticity, and NMR spectra.

The NMR-determined structures indicated a more highly ordered loop for the modified ASL^{Val3}_{UAC}, as compared to that of the unmodified ASL. The ASL^{Val3}_{UAC}-cmo^5U_{34};m^6A_{37} structure appears to be conformationally restrained. Furthermore, the free energy difference ($\Delta\Delta G°$) between modified and unmodified ASL^{Val3}_{UAC} was appreciably influenced by the entropy term ($\Delta\Delta S$), ~20 cal mol^{-1} K^{-1}. The hyperchromicity of ASL^{Val3}_{UAC}-cmo^5U_{34};m^6A_{37}, also a measure of order, was ~2-fold greater than that of the unmodified form. This clearly showed a contribution of the modifications to thermodynamic stability through ordering of the anticodon loop. Numerous posttranscriptional modifications have been found at the conserved purine 37, 3′-adjacent to the anticodon, as well as at wobble position 34. It was predicted that modification of purine 37 would maintain the all-important open anticodon loop structure for codon binding by negating intraloop hydrogen bonding but at the same time contribute order through enhanced base stacking (*9*). The presence of the modification N^6-isopentenyladenosine, i^6A_{37}, in *E. coli* ASL^{Phe} reduced the T_m and enhanced a low-temperature transition as opposed to its unmodified counterpart (*38*). Similar changes in thermal stability were observed in constructs of yeast ASL^{Phe} with three and four modifications (*4, 27*). The T_m value decreased due to the presence of m^1G_{37}. These studies confirmed that i^6A_{37} and m^1G_{37} negated intraloop hydrogen bonding and increased the level of base stacking. The anticodon loop of ASL^{Val3}_{UAC}-cmo^5U_{34};m^6A_{37} was wider than that of the unmodified ASL, indicating that either m^6A_{37}, cmo^5U_{34}, or both were maintaining the open loop. Considering what we know about other purine 37 modifications, m^6A_{37} may negate intraloop hydrogen bonding and may contribute to the base stacking in the loop of ASL^{Val3}_{UAC}. A statistical analysis of the local base step parameters (i.e., the tilt, the roll, and the twist angles) (*55*) of all the nucleotides of the two ASLs revealed that only the nucleotides of the loops differed significantly (see the Supporting Information). In particular, the angles of base tilt for the loop nucleotides of ASL^{Val3}_{UAC}-cmo^5U_{34};m^6A_{37} were considerably smaller than that of the unmodified ASL. The modified loop tilts averaged less than half that of the unmodified loop. The reduced step parameters of the loop nucleotides indicate again that the modifications of ASL^{Val3}_{UAC}-cmo^5U_{34};m^6A_{37} have an ordered loop through base stacking. This increase in order was not due solely to the added NOEs provided by the methyl group of m^6A_{37} since no such order was observed in the step parameters of the loop nucleosides of the singly modified ASL^{Val3}_{UAC}-m^6A_{37} (F. A. P. Vendeix et al., personal communication). Though the enhanced base stacking could result from the steric hindrance of the hydrophobic methyl group of m^6A_{37}, cmo^5U_{34} appears to be the major contributor. The increase in the level of base stacking may be achieved by $\pi-\pi$ interactions and hydrogen bonding of cmo^5U_{34}, the modification of which constrained its sugar pucker toward the C3′-*endo* conformation, and supported a π-like turn.

Anticodon π- or U-Turn Motif. Torsion angles, distance restraints, and NOE connectivities implicated the involvement of U_{33} in a π-like turn, though not all NMR criteria were met. However, the turn at U_{33} was more distinct in the ASL^{Val3}_{UAC}-cmo^5U_{34};m^6A_{37} structure than in the unmodified ASL. The NOE cross-peak between U_{33} H1′ and A_{35} H8 was higher in intensity in the modified ASL. A π-turn was identified in the anticodon and T loop regions of yeast $tRNA^{Phe}$ (*48*). In this anticodon loop region, the π-turn occurred at the 3′-phosphate of the invariant nucleotide, U_{33}, which was stacked with the semi-invariant 2′-*O*-methylcytidine 32 (Cm_{32}). At the wobble position, Gm_{34} was displaced

by the π-turn with angles α and ζ adopting the *trans* and g^- conformations, respectively. This distortion induced G_{34} P to stack with U_{33}. The imino proton of U_{33} was bound to the oxygen of its 3′-phosphate. As in $tRNA^{Phe}$ and other tRNAs, the modified ASL^{Val3}_{UAC} structure exhibited most, but not all, of the features characterizing the canonical U-turn. In particular, the expected NOE connectivities between U_{33} H2′ and the aromatic protons of U_{34} and A_{35} could not be observed. The addition of 5 mM Mg^{2+} did not alter the NMR spectra, indicating that the absence of the canonical U-turn was not due to the lack of the divalent ion. The presence of modifications at positions 37 and/or 34 per se does not induce a U-turn, although the chemical shift of the U_{33} 3′-phosphate was shifted downfield (*4, 38*). The anticodon loop of the elongator $tRNA^{Met}_{CAU}$ (*52*) has a base composition similar to that of ASL^{Val3}_{UAC}. The only difference is the anticodon base sequence. Although modifications were absent from the loop of ASL^{Met}_{CAU}, a U-turn was clearly identified (*52*). Thus, canonical turns could be observed in the absence or presence of modified bases in the loop of an ASL. However, specific combinations of modified bases in the loop generate a conformational restriction that could compel the ASL toward a U-turn conformation, for example, the fully modified ASL^{Lys} (*39, 56*).

Structural and Functional Contribution of m^6A_{37}. The highly conserved modification of purine 37 has expanded our concept of codon recognition beyond that of the three codon−anticodon interactions (*9*), invoking the "expanded anticodon" hypothesis (*3, 26, 57, 58*). The degree of hydrophobicity of the purine 37 modifications is associated with the stability of anticodon−codon base pairing (*9*). Analysis of the NMR and X-ray-derived structures showed that m^6A_{37} is probably negating intraloop base pairing and, thus, widening the anticodon loop. This modification reinforced the stability of the anticodon−codon minihelix by cross-strand stacking above the first adjacent codon base pair in the crystal structure (*46*), as did N^6-threonylcarbamoyladenosine, t^6A_{37} in ASL^{Lys} (*12*). However, the geometry of m^6A_{37} differs in cross-strand base stacking from that of t^6A_{37}, as seen in a comparison of the crystal structure of ASL^{Val3}_{UAC}-cmo^5U_{34};m^6A_{37} (*46*) with that of ASL^{Lys}_{UUU}-mnm^5U_{34};t^6A_{37} (*12*) bound to their respective codons. The two modifications are markedly different in size, and the t^6A_{37} ureido group acts as a third ring expanding its availability to stack with the adjacent base. The $tRNA^{Lys}_{UUU}$ anticodon−codon interaction is composed entirely of U-A base pairs which are less thermodynamically stable than C-G pairs (*48*). The unmodified ASL^{Lys}_{UUU} binds its cognate codon poorly as compared to ASL^{Lys}_{UUU}-t^6A_{37}, whereas the unmodified $tRNA^{Val3}_{UAC}$ binds its cognate codon in which the first base pair is C_{36}-G1 with an affinity similar to that of the modified ASL.

Modifications Order tRNA's Anticodon Domain. In his wobble hypothesis, Crick postulated that the ribosome would conform, remodel in today's terms, the anticodon to the codon (*10*). In contrast, the modified wobble hypothesis proposed that modifications restrain the anticodon domain conformation for accurate and effective reading of cognate and wobble codons (*11*). The solution structures presented here together with our recently published crystal structures of ASL^{Val3}_{UAC}-cmo^5U_{34};m^6A_{37} in complex with its four valine codons in the decoding site of the 30S ribosomal subunit (*46*) (resolution of 2.8−3.1 Å) provide us with the opportunity to test the two hypotheses. The doubly modified ASL^{Val3}_{UAC} employed in the solution studies and that used in the ribosome crystallization processes originated from the identical sample and at the same purity. The presence of the modified bases cmo^5U_{34} and m^6A_{37} in ASL^{Val3}_{UAC} was detected by the unbiased Fourier difference maps of ASL^{Val3}_{UAC}-cmo^5U_{34};m^6A_{37} bound to the cognate codon GUA, the wobble codon GUG, and GUU and GUC. The crystal structures of ASL^{Val3}_{UAC}-cmo^5U_{34};m^6A_{37} bound to the four codons were essentially identical. In addition, the superposition of the NMR and the crystal structure of ASL^{Val3}_{UAC}-cmo^5U_{34};m^6A_{37} exhibited considerable similarities with few significant noticeable differences. For the most part, the bases in the loop adopted the same orientation and stacking patterns with a rmsd of 2.30 ± 0.02 Å (Figure 9). As observed in the solution structure of the doubly modified ASL^{Val3}_{UAC}, the crystal structure on the ribosome displayed a high level of base stacking and order. At the top of the anticodon loop, A_{38} NH_2 was only 3.04 ± 0.22 Å from C_{32} O2, suggesting the probable formation of an intraloop A_{38}-C_{32} noncanonical base pair as observed in the solution structure (Figure 9). The backbone of the ASL loop in solution appears to be slightly wider than that in the crystal structure. This discrepancy in loop size could be attributed to bulk solvent differences between the solution and ribosome crystal states that influence the backbone dynamics. Also, the Mg^{2+} ion concentrations used during crystallization may contribute to phosphate backbone shielding. As a result, a more compact loop is obtained. This is not the case in the bulk solvent where effective ion shielding was achieved mostly by monovalent Na^+ and K^+.

Both the solution and crystal structures of the ASL had an abrupt turn at the wobble position (Figure 9). The ASL in the four crystal structures exhibited the canonical U-turn but also displayed an additional hydrogen bond that must be unique to xo^5U_{34} modifications. All three hydrogen bonds defining the presence of a canonical U-turn, U_{33} N3H···U_{36} O2P, U_{33} O2′···A_{35} N7, and A_{35} NH_2···U_{33} O2′, were observed in the crystals (*46*). However, the invariant U_{33} O2′ within all four crystal structures was also within hydrogen bonding distance (3.04 ± 0.20 Å) of the ether oxygen (O5) of cmo^5U_{34}. Though the U_{33} O2′−cmo^5U_{34} O5 distance in the solution structure exceeded that of hydrogen bonding, the observation in the crystals is of particular interest with regard to the expanded decoding capabilities of tRNAs with xo^5U_{34} (*46*). The U-turn and π-like turn hydrogen bonding within the crystal and solution structures of the modified ASL provided more stability to the turn by restraining the anticodon dynamics. A low variation of standard deviation was found for U_{33} N3···U_{36} O2P, U_{33} O2′···A_{35} N7, and A_{35} N6···C_{32} O2 hydrogen bonds, indicating a positional restraint of these bases as opposed to cmo^5U_{34} for which a slight repositioning is observed between the unbound and codon-bound structures. Obviously, only a subtle remodeling of the anticodon wobble position cmo^5U_{34} relative to U_{33} has occurred upon A-site binding.

The conformation of cmo^5U_{34} whether in the ASL^{Val3}_{UAC}-cmo^5U_{34};m^6A_{37} structure in solution or in the crystal contrasted sharply with the conformation found for the mononucleoside 5′-phosphate in solution. cmo^5U_{34} adopted the C3′-*endo* pucker conformation in the solution structure of the ASLs and in all four crystal structures of ASL^{Val3}_{UAC}-

cmo^{5}U$_{34}$;m^{6}A$_{37}$. In contrast, the mononucleoside 5′-phosphate of cmo^{5}U (and other oxy^5 derivatives, pxo^{5}U) in solution adopted the C2′-*endo* form which was not observed when the 5′-phosphate group was removed (*15*). Neither ASL$^{Val3}_{UAC}$-cmo^{5}U$_{34}$ in solution nor ASL$^{Val3}_{UAC}$-cmo^{5}U$_{34}$;m^{6}A$_{37}$ in the four crystals exhibited a hydrogen bond between cmo^5 and the nucleoside's 5′-PO$_4$ group. In contrast to the solution and crystal structures of the ASLs, the conformations of the xo^{5}U mononucleotides indicated that the 5-substituent was interacting with the 5′-phosphate (*15*). Thus, a cautious deduction of modified nucleoside/nucleotide contributions to RNA structure is warranted in interpreting modified mononucleoside and mononucleotide conformations.

CONCLUSION

After four decades of investigation, we are beginning to establish the critical chemical and physical contributions of modified nucleotides to the biology of tRNA's decoding of the genome (*9*). Crick postulated in the wobble hypothesis that the first two base pairs, and in some cases the third base pair, between tRNA's anticodon and the mRNA codon would be canonical, that pyrimidine-pyrimidine base pairs would not occur, and that the ribosome would conform the anticodon to the demands of the codon (*10*). He also proposed that G$_{34}$ was able to form a noncanonical base pair with U3, and vice versa, and that the purine I$_{34}$ would pair with U, C,and A, thus expanding the ability of tRNA to read multiple codons. Following this hypothesis, studies *in vitro* and *in vivo* (*14–16, 18, 44*) demonstrated that tRNAs with cmo^{5}U$_{34}$ were able to pair with A and G, but also with U and C. The enhanced hyperchromicities derived from the UV-monitored thermal transitions processes, the increased ellipticities of the CD spectra, the base stacking and base step parameters observed in the solution structures,and their comparison to X-ray analyses all indicate that modifications order and,thus, prestructure the anticodon domain. NMR relaxation studies of stable isotope-labeled ASLs should corroborate this conclusion. The A-site entry of a tRNA with an unmodified U$_{34}$ and an unstructured anticodon domain would impart an energetic penalty to codon binding that the ribosome would need to overcome to yield a productive pairing. In contrast, a modified U$_{34}$ in prestructuring the anticodon would not require the ribosome to invest in remodeling the anticodon. These and previous observations clearly suggest that the distinctive chemistry, structure,and dynamics of the modification at position 34 together with those at purine 37 achieve either a restricted or an expanded codon reading through an entropically derived loop structure that relieves the ribosome from having to remodel the anticodon.

ACKNOWLEDGMENT

We thank Dr. Glenn Björk for the HPLC analyses, Dr. Hanna Gracz for her technical support at the North Carolina State University NMR facility, and Mr. Song-oh Han and Ms. Virginia Moye for their contributions to the UV and CD experiments.

SUPPORTING INFORMATION AVAILABLE

Superposition of the ^{1}H−^{31}P HETCOR spectra of ASL$^{Val3}_{UAC}$ and ASL$^{Val3}_{UAC}$-cmo^{5}U$_{34}$;m^{6}A$_{37}$ (Figure 1), anomeric to aromatic NOE connectivity for ASL$^{Val3}_{UAC}$ and ASL$^{Val3}_{UAC}$-cmo^{5}U$_{34}$;m^{6}A$_{37}$ (Figure 2), local base step parameters of unmodified ASL$^{Val3}_{UAC}$ (Figure 3), and local base step parameters of ASL$^{Val3}_{UAC}$-cmo^{5}U$_{34}$;m^{6}A$_{37}$ (Figure 4). This material is available free of charge via the Internet at http://pubs.acs.org.

REFERENCES

1. Rich, A. (1977) Three-dimensional structure and biological function of transfer RNA. *Acc. Chem. Res. 10*, 388–402.
2. Kim, S. H. (1978) Three-dimensional structure of transfer RNA and its functional implications. *Adv. Enzymol. Relat. Areas Mol. Biol. 46*, 279–315.
3. Agris, P. F. (1996) The importance of being modified: Roles of modified nucleosides and Mg^{2+} in RNA structure and function. *Prog. Nucleic Acid Res. Mol. Biol. 53*, 79–129.
4. Stuart, J. W., Koshlap, K. M., Guenther, R., and Agris, P. F. (2003) Naturally-occurring modification restricts the anticodon domain conformational space of tRNA^{Phe}. *J. Mol. Biol. 334*, 901–918.
5. Lim, V. I. (1994) Analysis of action of wobble nucleoside modifications on codon-anticodon pairing within the ribosome. *J. Mol. Biol. 240*, 8–19.
6. Yarian, C., Townsend, H., Czestkowski, W., Sochacka, E., Malkiewicz, A. J., Guenther, R., Miskiewicz, A., and Agris, P. F. (2002) Accurate translation of the genetic code depends on tRNA modified nucleosides. *J. Biol. Chem. 277*, 16391–16395.
7. Urbonavicius, J., Qian, Q., Durand, J. M., Hagervall, T. G., and Björk, G. R. (2001) Improvement of reading frame maintenance is a common function for several tRNA modifications. *EMBO J. 20*, 4863–4873.
8. Urbonavicius, J., Stahl, G., Durand, J. M., Ben Salem, S. N., Qian, Q., Farabaugh, P. J., and Björk, G. R. (2003) Transfer RNA modifications that alter +1 frameshifting in general fail to affect−1 frameshifting. *RNA 9*, 760–768.
9. Agris, P. F., Vendeix, F. A., and Graham, W. D. (2007) tRNA's wobble decoding of the genome: 40 years of modification. *J. Mol. Biol. 366*, 1–13.
10. Crick, F. H. (1966) Codon−anticodon pairing: The wobble hypothesis. *J. Mol. Biol. 19*, 548–555.
11. Agris, P. F. (1991) Wobble position modified nucleosides evolved to select transfer RNA codon recognition: A modified-wobble hypothesis. *Biochimie 73*, 1345–1349.
12. Murphy, F. V., Ramakrishnan, V., Malkiewicz, A., and Agris, P. F. (2004) The role of modifications in codon discrimination by tRNA$^{Lys}_{UUU}$. *Nat. Struct. Mol. Biol. 11*, 1186–1191.
13. Ishikura, H., Yamada, Y., and Nishimura, S. (1971) Structure of serine tRNA from *Escherichia coli*. I. Purification of serine tRNA's with different codon responses. *Biochim. Biophys. Acta 228*, 471–481.
14. Mitra, S. K., Lustig, F., Akesson, B., Axberg, T., Elias, P., and Lagerkvist, U. (1979) Relative efficiency of anticodons in reading the valine codons during protein synthesis in vitro. *J. Biol. Chem. 254*, 6397–6401.
15. Yokoyama, S., Watanabe, T., Murao, K., Ishikura, H., Yamaizumi, Z., Nishimura, S., and Miyazawa, T. (1985) Molecular mechanism of codon recognition by tRNA species with modified uridine in the first position of the anticodon. *Proc. Natl. Acad. Sci. U.S.A. 82*, 4905–4909.
16. Sørensen, M. A., Elf, J., Bouakaz, E., Tenson, T., Sanyal, S., Björk, G. R., and Ehrenberg, M. (2005) Over expression of a tRNA^{Leu} isoacceptor changes charging pattern of leucine tRNAs and reveals new codon reading. *J. Mol. Biol. 354*, 16–24.
17. Sprinzl, M., and Vassilenko, K. S. (2005) Compilation of tRNA sequences and sequences of tRNA genes. *Nucleic Acids Res. 33*, D139−D140.
18. Nasvall, S. J., Chen, P., and Björk, G. R. (2004) The modified wobble nucleoside uridine-5-oxyacetic acid in tRNA^{Pro}(cmo^{5}UGG) promotes reading of all four proline codons in vivo. *RNA 10*, 1662–1673.
19. Phelps, S. S., Malkiewicz, A., Agris, P. F., and Joseph, S. (2004) Modified nucleotides in tRNA^{Lys} and tRNA^{Val} are important for translocation. *J. Mol. Biol. 338*, 439–444.
20. Scaringe, S. A., Wincott, F. E., and Caruthers, M. H. (1998) Novel RNA Synthesis Method Using 5′-Silyl-2′-Orthoester Protecting Groups. *J. Am. Chem. Soc. 120*, 11820–11821.
21. Boudou, V., Van Aerschot, A., Hendrix, C., Millar, A., Weiss, P., and Herdewijn, P. (2000) Synthesis of the anticodon hairpin

tRNA^{fMet} containing N-{[9-(β-D-ribofuranosyl)-9H-purin-6-yl]carbamoyl}-L-threonine-N6-{{[(1S,2R)-1-carboxy-2-hydroxypropyl]-amino}-carbonyl} adenosine, (t6A). *Helv. Chim. Acta 83*, 152–161.
22. Gehrke, C. W., Kuo, K. C., McCune, R. A., Gerhardt, K. O., and Agris, P. F. (1982) Quantitative enzymatic hydrolysis of tRNAs: Reversed-phase high-performance liquid chromatography of tRNA nucleosides. *J. Chromatogr. 230*, 297–308.
23. Fahlman, R. P., Dale, T., and Uhlenbeck, O. C. (2004) Uniform binding of aminoacylated transfer RNAs to the ribosomal A and P sites. *Mol. Cell 16*, 799–805.
24. Zuker, M. (2003) Mfold web server for nucleic acid folding and hybridization prediction. *Nucleic Acids Res. 31*, 3406–3415.
25. Ericson, G., Minchew, P., and Wollenzein, P. (1995) Structural changes in base-paired region 28 in 16 S rRNA close to the decoding region of the 30S ribosomal subunit are correlated to changes in tRNA binding. *J. Mol. Biol. 250*, 407–419.
26. Wong, I., and Lohman, T. M. (1993) A double-filter method for nitrocellulose-filter binding: application to protein-nucleic acid interactions. *Proc. Natl. Acad. Sci. U.S.A. 90*, 5428–5432.
27. Ashraf, S. S., Guenther, R. H., Ansari, G., Malkiewicz, A., Sochacka, E., and Agris, P. F. (2000) Role of modified nucleosides of yeast tRNA^{Phe} in ribosomal binding. *Cell Biochem. Biophys. 33*, 241–252.
28. Serra, M. J., and Turner, D. H. (1995) Predicting thermodynamic properties of RNA. *Methods Enzymol. 259*, 242–261.
29. Delaglio, F., Grzesiek, S., Vuister, G. W., Zhu, G., Pfeifer, J., and Bax, A. (1995) NMRPipe: A multidimensional spectral processing system based on UNIX pipes. *J. Biomol. NMR 6*, 277–293.
30. Goddard, T. D., and Kneller, D. G. (2007) SPARKY3, University of California, San Francisco.
31. Piotto, M., Saudek, V., and Sklenar, V. (1992) Gradient-tailored excitation for single-quantum NMR spectroscopy of aqueous solutions. *J. Biomol. NMR 2*, 661–665.
32. Kumar, A., Ernst, R. R., and Wuthrich, K. (1980) A two-dimensional nuclear Overhauser enhancement (2D NOE) experiment for the elucidation of complete proton-proton cross-relaxation networks in biological macromolecules. *Biochem. Biophys. Res. Commun. 95*, 1–6.
33. Bax, A., and Davis, D. G. (1985) MLEV-17-based two dimensional homonuclear magnetization transfer spectroscopy. *J. Magn. Reson. 65*, 355–360.
34. Brunger, A. T., Adams, P. D., Clore, G. M., DeLano, W. L., Gros, P., Grosse-Kunstleve, R. W., Jiang, J. S., Kuszewski, J., Nilges, M., Pannu, N. S., Read, R. J., Rice, L. M., Simonson, T., and Warren, G. L. (1998) Crystallography & NMR system: A new software suite for macromolecular structure determination. *Acta Crystallogr. D54*, 905–921.
35. Varani, G., Abdoul-ela, F., and Allain, F. H-T. (1996) NMR investigation of RNA structure. *Prog. Nucl. Magn. Reson. Spectrosc. 29*, 51–127.
36. Varani, G., and Tinoco, I., Jr. (1991) RNA structure and NMR spectroscopy. *Q. Rev. Biophys. 24*, 479–532.
37. Stein, E. G., Rice, L. M., and Brunger, A. T. (1997) Torsion-angle molecular dynamics as a new efficient tool for NMR structure calculation. *J. Magn. Reson. 124*, 154–164.
38. Cabello-Villegas, J., Winkler, M. E., and Nikonowicz, E. P. (2002) Solution conformations of unmodified and A(37)N(6)-dimethylallyl modified anticodon stem-loops of *Escherichia coli* tRNA^{Phe}. *J. Mol. Biol. 319*, 1015–1034.
39. Durant, P. C., Bajji, A. C., Sundaram, M., Kumar, R. K., and Davis, D. R. (2005) Structural effects of hypermodified nucleosides in the *Escherichia coli* and human tRNA^{Lys} anticodon loop: The effect of nucleosides s^2U, mcm^5U, mcm^5s^2U, mnm^5s^2U, t^{6A}, and ms^2t^6A. *Biochemistry 44*, 8078–8089.
40. Fasman, G. D. (1996) *Circular Dichroism and the Conformational Analysis of Biomolecules*, Plenum Press, New York.
41. Chen, Y., Sierzputowska-Gracz, H., Guenther, R., Everett, K., and Agris, P. F. (1993) 5-Methylcytidine is required for cooperative binding of Mg^{2+} and a conformational transition at the anticodon stem-loop of yeast phenylalanine tRNA. *Biochemistry 32*, 10249–10253.
42. Gabriel, K., Schneider, J., and McClain, W. H. (1996) Functional evidence for indirect recognition of G.U in tRNA^{Ala} by alanyl-tRNA synthetase. *Science 271*, 195–197.
43. Kothe, U., and Rodnina, M. V. (2007) Codon reading by tRNA^{Ala} with modified uridine in the wobble position. *Mol. Cell 25*, 167–174.
44. Nasvall, S. J., Chen, P., and Björk, G. R. (2007) The wobble hypothesis revisited: Uridine-5-oxyacetic acid is critical for reading of G-ending codons. *RNA 13*, 2151–2164.
45. Ogle, J. M., Murphy, F. V., Tarry, M. J., and Ramakrishnan, V. (2002) Selection of tRNA by the ribosome requires a transition from an open to a closed form. *Cell 111*, 721–732.
46. Weixlbaumer, A., Murphy, F. V., Dziergowska, A., Malkiewicz, A., Vendeix, F. A., Agris, P. F., and Ramakrishnan, V. (2007) Mechanism for expanding the decoding capacity of transfer RNAs by modification of uridines. *Nat. Struct. Mol. Biol. 14*, 498–502.
47. Wijmenga, S. S., and van Buuren, B. N. M. (1998) The use of NMR methods for conformational studies of nucleic acids. *Prog. Nucl. Magn. Reson. Spectrosc. 32*, 287–387.
48. Saenger, W. (1983) *Principles of Nucleic Acid Structure*, Springer-Verlag, New York.
49. Fissekis, J. D., and Sweet, F. (1970) Synthesis of 5-carboxymethyluridine. A nucleoside from transfer ribonucleic acid. *Biochemistry 9*, 3136–3142.
50. Takai, K., and Yokoyama, S. (2003) Roles of 5-substituents of tRNA wobble uridines in the recognition of purine-ending codons. *Nucleic Acids Res. 31*, 6383–6391.
51. Hilal, S. H., Karickhoff, S. W., and Carreira, L. A. (1995) A rigorous test for SPARC's chemical reactivity models: Estimation of more than 4300 ionization pKa's. *Quant. Struct.−Act. Relat. 14*, 348–355.
52. Schweisguth, D. C., and Moore, P. B. (1997) On the conformation of the anticodon loops of initiator and elongator methionine tRNAs. *J. Mol. Biol. 267*, 505–519.
53. Vermeulen, A., McCallum, S. A., and Pardi, A. (2005) Comparison of the global structure and dynamics of native and unmodified tRNA^{Val}. *Biochemistry 44*, 6024–6033.
54. Durant, P. C., and Davis, D. R. (1999) Stabilization of the anticodon stem-loop of tRNALys,3 by an A+-C base-pair and by pseudouridine. *J. Mol. Biol. 285*, 115–131.
55. Lu, X. J., and Olson, W. K. (2003) 3DNA: A software package for the analysis, rebuilding and visualization of three-dimensional nucleic acid structures. *Nucleic Acids Res. 31*, 5108–5121.
56. Stuart, J. W., Gdaniec, Z., Guenther, R., Marszalek, M., Sochacka, E., Malkiewicz, A., and Agris, P. F. (2000) Functional anticodon architecture of human tRNA^{Lys3} includes disruption of intraloop hydrogen bonding by the naturally occurring amino acid modification, t6A. *Biochemistry 39*, 13396–13404.
57. Yarus, M. (1982) Translational efficiency of transfer RNA's: Uses of an extended anticodon. *Science 218*, 646–652.
58. Olejniczak, M., and Uhlenbeck, O. C. (2006) tRNA residues that have coevolved with their anticodon to ensure uniform and accurate codon recognition. *Biochimie 88*, 943–950.

BI702356J